Nemens *et al. Fire Ecology* (2026) 22:92
https://doi.org/10.1186/s42408-026-00503-6

Fire Ecology

RESEARCH

Open Access

# Quantifying understory fuel structure and biomass using coupled terrestrial lidar scanning, close-range photogrammetry, and field sampling

Deborah G. Nemens[1*], Susan J. Prichard[1], Gina R. Cova[1], Brian Drye[1], Paige Eagle[1], Eric Rowell[2] and Jessie Thoreson[1]

## Abstract

**Background** We evaluated the three-dimensional (3D) structure, composition, and biomass of understory fuels common to prescribed burn programs in pine-dominated forests of the southeastern and western United States. Traditional fuel characterization in these systems has been limited to two-dimensional representations, including biomass, height, and cover estimates per unit area. The objective of this study was to compare close-range photogrammetry with terrestrial lidar scanning (TLS), validated by destructive sampling to inform gridded 3D maps of live and dead understory fuels.

**Results** We developed and analyzed a large dataset of calibrated plots using co-located terrestrial lidar scanning (TLS), close-range photogrammetry, and destructive biomass sampling conducted at 18 field sites across the southeastern and western US. Field sites represented vegetation commonly burned in prescribed fire programs, including southeastern mesic flatwood forests, southeastern loblolly-sweetgum forests, western ponderosa pine and mixed conifer forests, and western grasslands. Scanning methods were compared with metrics derived from fine-scale volumetric fuels sampling to determine the most effective method for mapping fuels in 3D. TLS and SfM-based point cloud metrics were variable in their accuracy dependent on vegetation type and levels of occlusion in understory vegetation, and neither was effective at predicting fuels within the lowest sampled stratum (0–10 cm).

**Conclusions** Modeled relationships between photogrammetry and TLS-based metrics and fuel biomass and bulk density can be used to produce unit-scale mapping for prescribed burn programs that are informed by the 3D structure and composition of understory fuels. However, point-cloud metrics may be limited in their utility in dense fuel complexes with high levels of occlusion. This work supports advances in the characterization and mapping of wildland fuel beds for use in physics-based models of fire behavior and effects that rely on gridded, 3D inputs.

## Resumen

**Antecedentes** Evaluamos tridimensionalmente (3D) la estructura, composición, y biomasa de combustibles de sotobosques comunes en los programas de quemas prescriptas en bosques dominados por pinos del sudeste y del oeste

*Correspondence:
Deborah G. Nemens
dnemens@uw.edu
Full list of author information is available at the end of the article

de los EEUU. La caracterización tradicional en esos sistemas ha estado limitada a representaciones bidimensionales, incluyendo biomasa, altura, y estimaciones de cobertura por área. El objetivo de este estudio fue comparar la fotogrametría de corto rango (o alcance) con el escaneo terrestre por LIDAR (TLS), validados por muestreos destructivos, para informarlos en mapas en 3D de combustibles vivos y muertos del sotobosque.

**Resultados** Desarrollamos y analizamos una gran base de datos de parcelas calibradas usando en las mismas el escaneo terrestre LIDAR (TLS), la fotogrametría de corto alcance, y muestreos destructivos de la vegetación en 18 sitios a campo en el sudeste y oeste de los EEUU. Los sitios a campo representaron la vegetación que se quema comúnmente en programas de quemas prescriptas, incluyendo bosques mésicos de planicies del sudeste, bosques de pino taeda y liquidámbar del sudeste, bosques de pino ponderosa y mixtos de coníferas del oeste. Los métodos de escaneo fueron comparados con métricas derivadas el muestreo de datos volumétricos de combustibles a escala fina, para determinar el método más efectivo para mapear combustibles en 3D. Las métricas del TLS y las basadas en nubes de puntos SfM, resultaron variables en sus exactitudes, dependiendo del tipo de vegetación y de los niveles de oclusión de la vegetación del sotobosque, y ninguno fue efectivo en predecir los combustibles dentro del estrato medido más cerca de la superficie (0–10 cm).

**Conclusiones** Las relaciones modeladas entre fotogrametría y las métricas basadas en TLS y la biomasa combustible y la densidad aparente puede usarse para producir mapas a escala de unidades para programas de quemas prescriptas que sean informadas por la estructura 3D y la composición de los combustibles del sotobosque. Sin embargo, las métricas basadas en nubes de puntos pueden estar limitadas en su utilidad en complejos de combustibles densos o con grandes niveles de oclusión. Este trabajo respalda los avances en la caracterización y mapeo de camas de combustibles vegetales para su uso en modelos físicos de comportamiento del fuego que se basan en aportes de grillas 3D.

## Introduction

The structure and composition of forests are relevant for a range of management applications, including forest mensuration, biomass and carbon inventories, wildlife habitat assessments, and potential fire behavior and effects. For wildland fire modeling and fuel treatment assessments, live and dead vegetation is often referred to as wildland fuelbeds or fuel complexes, representing the potential energy in live and dead biomass that can contribute to the preheating and ignition of adjacent fuels (Albini 1976; Keane 2015; Finney et al. 2021). Because wildland fuels are the product of vegetation growth, dieback, and disturbances (Keane 2015), they are highly dynamic over space and time. The structure and composition of vegetation not only influence fire ignition, spread, and heat release but also patterns of how air and fire move within wildland fire events. For example, trees and large shrubs can act as barriers to wind flow and thus influence the spread and duration of fire behavior (Pimont et al. 2016). Similarly, low branches can act as ladder fuels, allowing surface fire to transition into the tree canopy.

Understory vegetation, often referred to as surface fuel in wildland fire behavior models, is the primary driver of fire spread and energy transfer (Rothermel 1972; Keane 2015; Linn et al. 2020). Understory vegetation in this context refers to the seedlings, saplings, shrubs, and herbaceous plants growing under the forest canopy. Prescribed burning programs commonly target the understory to maintain fire-adapted vegetation and structure in southeastern (SE) and western US pine forests. Under moderate fire weather and fuel moisture conditions representative of most prescribed burn windows, the structure and composition of surface fuels are critical to predicting fire behavior (Hiers et al. 2009; Loudermilk et al. 2018, 2022). Even when forest canopies are consumed in crown fire events, fire behavior is generally still dependent on the intensity, duration, and spread of surface fire (Finney et al. 2021). The spatial configuration and composition of surface fuels are thus critical components of wildland fire behavior and effects but are often greatly oversimplified in models due to great uncertainty in model assumptions. Although fire and fuels managers are aware of how spatial variability in surface fuels influences fire behavior, higher resolution surface fuel characterization and mapping is required to guide prescriptions and burn management approaches (Hiers et al. 2009; Rowell et al. 2020; Atchley et al. 2021).

Surface fuels have traditionally been represented by two-dimensional (2D) characterization and mapping of biomass (kg m$^{-2}$) and depth (m) at coarse spatial scales in operational fire behavior modeling (Rothermel 1972). Next-generation fire behavior modeling offers improvements to traditional models, leveraging the increased availability of computing power and improved methods for generating gridded inputs of wind fields and fuels. These newer models, such as FIRETEC, FDS, and QUIC Fire (Linn et al. 2002, 2020; Mell et al. 2007) rely on 3D inputs of wildland fuel complexes comprised of both canopy and understory fuels (Hiers et al. 2009; Loudermilk et al. 2014).

The data demands of these next-generation fire models have spurred the development of novel methods for three-dimensional (3D) characterization and mapping of wildland fuels. Given the complexity of surface fuels and their importance to fire behavior, increased emphasis is being placed on techniques that can accurately characterize these fuels in wildland settings. The field is still in early stages, and methods for imagery collection and calibration for field development are under active study (Loudermilk et al. 2012; Bright et al. 2016; Rowell et al. 2020; Hudak et al. 2020) along with the sensitivity of physics-based models of fire behavior to the resolution and physical structure and characteristics of surface fuels (Mueller et al. 2021; Ganteaume et al. 2023).

One of the more established methods is terrestrial lidar scanning (TLS), which uses active sensors to create 3D point clouds of objects on a sub-centimeter scale. TLS has been extensively employed to produce metrics important to fire behavior models, such as fuel height, volume, and biomass (Rowell et al. 2020; Calders et al. 2020; Loudermilk et al. 2023; Tenny et al. 2025; Arcidiaco et al. 2026). However, this highly precise mapping technology requires access to expensive scanning equipment and considerable expertise to operate instruments and process data, presenting barriers to widespread use (Enterkine et al. 2025). Techniques such as structure-from-motion (SfM) photogrammetry offer a more accessible method, relying on more portable and inexpensive technologies, such as commonly used consumer-grade cameras and smartphones. SfM photogrammetry, like TLS, can produce 3D point clouds which in turn are used to produce critical fuel model inputs. Handheld SfM is a promising technique that can be used to characterize fuel height, volume, and surface area, and predict biomass (Bright et al. 2016; Wallace et al. 2017; Piermattei et al. 2019; Cova et al. 2023; Enterkine et al. 2025) but has not been evaluated as extensively as TLS, and comparison is warranted to assess its utility as a substitute technology. Specifically, more study is needed to determine the ability of SfM-derived metrics to accurately represent field measures of fuel characteristics, and whether products of this method are equal to those of more widely used TLS techniques.

The objectives of this study were to evaluate relationships between point cloud metrics derived from terrestrial lidar scanning (TLS) and SfM photogrammetry with co-located biomass sampling, and to assess the utility of each metric in informing fine-scale 3D maps of live and dead understory biomass in frequently burned pine-dominated forests of the SE and western United States. Fuel biomass, and its vertical and horizontal distribution, is a key input for fire behavior models, as it is highly consequential for behavior important to prescribed fire managers, such as flame residence times and quantity of smoke production (Prichard et al. 2019). Pine forests within the SE and western US are frequently targeted for treatment in prescribed burning programs and thus necessitate improved fuel characterization that is spatially explicit. Using field plots in which fuels were typed and destructively sampled in volumetric sampling cubes, we evaluated point cloud-based metrics from both methods to model fuel height, volume, and biomass across major fuel categories including timber litter, grass, and shrubs. We compared predictive models of surface fuel biomass based on individual point cloud metrics from TLS and close-range photogrammetry datasets. The central questions guiding this analysis are (1) how does inexpensive photogrammetry represent surface fuels when compared to higher-cost terrestrial laser scanning, and (2) how well do point cloud-derived metrics of height, volume, and surface area predict field-measured values of biomass? As TLS and SfM imagery become more accessible to managers, evaluation of modeled relationships between point cloud metrics and measured biomass are needed to inform how understory fuel complexes can be measured and modeled in 3D.

## Methods

This study is part of a larger research program using a hierarchical sampling approach to characterize the 3D structure and composition of forest and grassland fuels that are common to prescribed burning programs in the SE and western US (Prichard et al. in review). Although widely separated across the continent, forest sites are similar in structure, with open canopies dominated by mature trees and lower-stature forest understories, in most cases fire-maintained. Regional climate, productivity, and vegetation types markedly differ between SE and western sites and thus offer a way to evaluate how our sampling methods and fuel characterization can be used to characterize understory fuels across a range of fuel complexes from sites dominated by timber litter, grass, and shrub fuels. Specifically, SE sites are located within mesic flatwoods with a subtropical climate and high site productivity characterized by evergreen shrubs, bunchgrasses, and abundant pine needle litter, while western ponderosa pine sites have a semiarid climate and lower site productivity, with a greater preponderance of timber-litter and grass fuel complexes.

### Study sites

Eighteen sites were selected for this study (Table S2), including six sites located in SE pine forests with mesic flatwood understories (SE flatwood), three sites in SE loblolly plantation forests with sweetgum understories (SE loblolly-sweetgum), five western sites in semi-arid ponderosa pine and mixed conifer forests (Western pine), and four western grassland sites (Western grassland). Site specifications for forested areas included sites that (1) had relatively open (< 50% canopy cover), single-layered pine forest that allowed for UAS scanning as part of a coordinated study; (2) were located on relatively flat ground with < 20% slope gradient; and (3) had consistent management history (e.g., past thinning and burning was uniform across the site) and relatively uniform canopy and surface fuels. All sites were selected such that they consisted of a range of biomass values from low to high. In the SE, this was achieved by selecting sites with varying time since last fire (TSF), between 1 to 5 years. Lower productivity western sites, where prescribed fire use is less widespread, were chosen based on ocular estimations of biomass accumulation across a range of values, and these are reported in lieu of time since fire for these sites.

SE flatwoods sites, located in Georgia and northern Florida (Aucilla, Blackwater, Fort Stewart, Osceola, and Tates Hell A and B, Figs. 1 and 2, Table S2), have warm and humid climates, ranging in temperature from winter lows averaging 9.2 °C and summer highs averaging 31.1 °C. Annual precipitation in the region averages 134 cm, with more rain falling during the June–August growing season. Overstories are dominated by longleaf pine (*Pinus palustris* Mill) and slash pine (*Pinus elliottii* Engelm.) with occasional loblolly pine (*Pinus taeda* L.). Sites with shrub-dominated understories largely contain saw palmetto (*Serenoa repens* (W. Bartram) Small) and gallberry (*Ilex glabra* L.), with occasional deciduous shrubs such as blueberry (*Vaccinium* spp.). A few sites have grassy understories consisting of wiregrass (*Aristida stricta* Michx.) and assorted bunchgrasses.

SE loblolly-sweetgum sites (Hannah Hammock and Hitchiti A and B, Figs. 1 and 2, Table S2) are also located


**Fig. 1** Map of 3D Fuels project study site locations

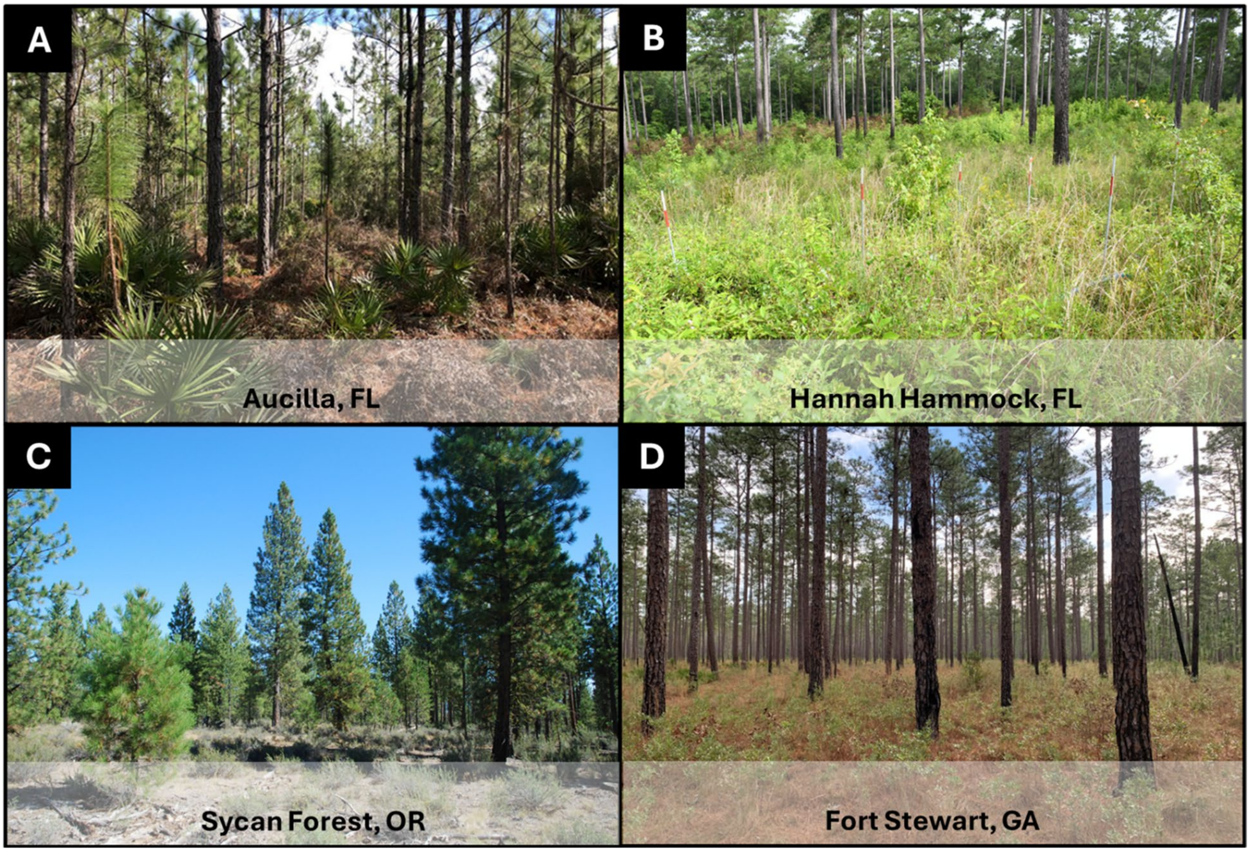


**Fig. 2** Representative site photos with high understory complexity and biomass (**A** and **B**), and comparatively low understory complexity and biomass (**C** and **D**)

in Georgia and Florida, with similar climates to the SE flatwoods sites. These sites are generally dominated by loblolly pine in the overstory, although slash pine and shortleaf pine (*Pinus echinata Mill.*) are also common. Understories contain a large component of sweetgum (*Liquidambar styraciflua* L.), as well as American beautyberry (*Callicarpa americana* L.), various shrub-form oak species (*Quercus* spp.), winged sumac (*Rhus copallinum* L.), and greenbriar (*Smilax* spp.).

Western pine sites (LANL Forest, Lubrecht, Methow, and Sycan Forest I and II, Figs. 1 and 2, Table S2) are located in semi-arid climates in Washington, Oregon, Montana, and New Mexico with average temperatures ranging from − 7.5 °C in January and a monthly maximum of 29.3 °C. Most precipitation falls as snow between November and March, and averages 36.5 cm annually. These are dominated by ponderosa pine (*Pinus ponderosa* Dougl. ex Laws.) in the overstory, with some Douglas-fir (*Pseudotsuga menziesii* (Mirb.) Franco). These have more open understories than SE sites, commonly consisting of scattered bitterbrush, kinnickinnick (*Arctostaphylos uva-ursi* (L.) Spreng.), and huckleberry (*Vaccinium* spp.) with some bunchgrasses and *Carex* spp. New Mexico sites also had a substantial component of shrubby gambel oak (*Quercus gambelii* Nutt.).

Western grassland sites in Washington and Oregon (Glacial Heritage, LANL grassland, Sycan Grassland and Tenalquot, Fig. 1, Table S2) are dominated by invasive species such as tall oatgrass (*Arrhenatherum elatius* (L.) P. Beauv. ex J. Presl & C. Presl), colonial bentgrass (*Agrostis stolonifera* L.), Scot's broom (*Cytisus scoparius* (L.) Link), hairy cat's ear (*Hypochaeris radicata* L.), and various annual grasses and forbs. Native species such as Roemer's fescue (*Festuca roemerii* (Pavlick) Alexeev), kinnickinnick, and bracken fern (*Pteridium aquilinum* (L.) Kuhn) are also present.

### Sampling design

The hierarchical sampling design employed in the larger project of which this study was a part includes synoptic TLS coverage of a 4000-$m^2$ unit within each site, higher-resolution TLS scans of 13 randomly selected (via random number generator) 5×5 m plots, and 0.5×0.5 × 1 m clip plots nested within 9 of these plots chosen for destructive sampling (Prichard et al., in review). For this study, we used data collected from 0.5×0.5 × 1 m clip plots. These were located within each of the 9 5×5 m plots selected for destructive sampling at 1 m from the NW, NE, SW, and SE corners and the center (CTR) of the plot. Prior to scanning and sampling, corners of 5×5 m plots were marked with metal conduit; clip plots were marked with conduit and a 0.5×0.5 m 2D PVC frame wrapped in reflective tape.

**Field sampling**

TLS scanning was conducted using a RIEGL VZ-2000 (RIEGL Deutschland Vertriebsgesellschaft mbH, Horn, Austria); a RIEGL VZ-400i was used when the VZ-2000 unit was unavailable to scan the Fort Stewart and Hitchiti A and B units. Both scanners had a sampling rate of 750 kHz with a scan line density of 0.21 degrees and were mounted on a tripod at 1.5 m in height. One TLS scan was collected at the midpoint of each side of selected 5×5 m plots, for a total of four overlapping scans per plot.

A handheld GoPro Hero 7 camera (GoPro, Inc., San Mateo, CA, USA) mounted on a rigid pole was used to collect imagery used in close-range photogrammetry models. Camera settings were set uniformly at 2700 k resolution, with a rate of 60 frames per second, using a linear camera angle and filming for 1–2 min. With the reflective 2D PVC frame still in place, each 0.5×0.5 clip plot was filmed individually using a snaking pattern, with 7 equally spaced passes that crossed the plot at an approximate height of 1 m; 7 additional passes were repeated at a $90^{0}$ angle to the initial pattern. Finally, each plot was circled at an oblique angle with the camera pointed inward before ending the video. In addition to the reflective 2D frame, printed black and white targets and pool noodles were placed around the plot as markers to aid in merging images together during later processing.

Clip plots were measured and destructively sampled using volumetric 0.5×0.5×1 m sampling frames (hereafter voxel frames) with a moveable 2D frame divided into 25 10 cm squares to conduct ocular presence/absence surveys and destructive sampling of fuels in gridded 0.1 $m^3$ voxel space (following methods in Hawley et al. 2018). The voxel frame was constructed of PVC pipe and was designed to be placed over the precise location of the reflective 2D frames (which were removed before sampling) used to delineate clip plots during scanning. For each clip plot, presence or absence for each of 19 predetermined categories (see Prichard et al. in review for details) was recorded for each 10×10-cm voxel, and all biomass was then subsequently collected for each 10-cm vertical stratum (e.g., 20–30 cm), starting from the highest stratum where fuels were present and continuing until mineral soil was encountered. Each stratum was clipped and bagged separately for laboratory analysis, as was any duff encountered below litter layers.

Biomass samples were oven dried in the laboratory for a minimum of 48 h. at 70 °C and weighed. Samples collected from the lowest (0–10 cm) stratum were sorted by the same fuel categories as above, each of which was dried and weighed separately. Before analysis, these categories were sorted into coarse fuel types: shrub, herb and timber litter. Biomass samples taken from above 10 cm were not sorted into fuel types and were dried and weighed by stratum alone (i.e., 20–30 cm, 30–40 cm). Duff biomass values were also quantified, but removed from plot biomass calculations before analysis, as this fuel element is not captured in remote sensing point clouds.

**Image processing**

TLS scans were registered and georeferenced using RiSCAN PRO (www.riegl.com; Horn, Austria) and then exported as laz files for further processing. The LAStools *lasmerge* function (https://rapidlasso.de; Gilching, Germany) was used to merge the 4 scans collected at the 5×5 m plots into a single point cloud, and the *normalize_height* function in the LidR package in the R statistical software program (Roussel et al. 2020) was used to normalize the merged point clouds. The point clouds of each voxel plot were clipped from these files using a custom shiny tool (detailed methods available on the 3D Fuels data repository: https://doi.org/10.60594/W4W016, tool available in code repository: https://github.com/uw-flame-lab/3D_Fuels_PUBLIC/) that utilized the reflectivity of conduit poles and 2D squares installed prior to scanning to identify the 0.5×0.5×1 m clip plot boundaries. This tool created a laz file for each clip plot, as well as shapefile points and polygons representing the reflective pole locations and the 2D outline of the plot on the ground surface, respectively.

Close-range structure-from-motion photogrammetry point clouds were created from GoPro videos following a workflow combining automated scripts with manual processing. Custom Python scripts (detailed methods available on the 3D Fuels data repository: https://doi.org/10.60594/W4W016, scripts available in code repository: https://github.com/uw-flame-lab/3D_Fuels_PUBLIC/) were used to parse each video into a set of approximately 400 still images. Irrelevant images (such as those that did not capture the 2D reflective frames, blurry images, or images of the ground or sky at the end of each video) were manually screened and discarded. Agisoft Metashape Pro (Version 1.6, Agisoft LLC., www.agisoft.com, accessed January 2023) was used to create 3D representations of each plot from the set of still images. The software relies on the automatic detection of “markers,” which are easily detectable, shared points across a set of images (such as corners of 2D frames, pool noodles or printed targets placed before filming) that are used to tie images together into a point cloud. In the creation of point clouds, we used the following parameters: photo alignment accuracy was set to "high," depth map quality was set to "medium," and depth filtering was "mild," following recommendations (E. Rowell pers comm). If the software could not detect these common points automatically, markers were identified manually by a technician, and models were re-created. Each point cloud was trimmed to the dimensions of the clip plot in Cloud Compare (Version 2.13, https://cloudcompare.org, accessed March 2023) using the dimensions of the shapefile polygons generated from the TLS clipping process. Images of TLS and SfM point clouds, as well as high-resolution photos of each plot, are available online at https://depts.washington.edu/fft/plotviewer/index.html.

#### Point-cloud metrics

Co-located and clipped TLS and SfM point clouds were used to develop a set of metrics that could be compared with field-derived metrics from destructive voxel plot data, following the methodology used in Cova and others (2023). Occupied volume was determined for each clip plot using the voxR package (Lecigne et al. 2018) in R to segment each point cloud into 10 $cm^3$ voxels, as this was the unit of occupancy used in the field data collection effort. This value was then divided by the total possible number of voxels in a clip plot (250) to calculate a percentage of total voxel-based volume occupied for each point cloud. Height was determined by the mean height of the point cloud based on segmentation of the plot into individual $10 \times 10$ cm columns of voxels, where the 99th percentile height value of all points was calculated for each voxel column (25 per plot) and averaged across the plot. Projected area density (PAD) and vertical projected area density (PADV) were calculated using voxel occupancy in the $x$ and $y$ and $x$ and $z$ dimensions, respectively. PAD is akin to a top-down view of the clip plot, while PADV is like a side view of the plot, both of which summarize the 3D occupied space in 2 gridded dimensions. Surface area (SA) and volume (Vol) for each plot were calculated from a convex hull created by draping a minimum-bounding shell over all points in the point cloud using the 'convhulln' function in the geometry package in R. Points below 10 cm in height were excluded from the hull in order to avoid using ground points in these calculations.

#### Field metrics

Summary data from ocular surveys were used to calculate a maximum height for each plot, defined as the highest strata which contained vegetation as recorded during surveys. Mean height was calculated by taking the tallest vegetation in each voxel column and averaging those heights across the plot. Occupied volume was calculated for each plot by dividing the total number of voxels recorded as containing fuel by the total number of possible voxels in each plot (250). Dry weight biomass was summarized by plot, 10-cm vertical stratum (0–10 through 90–100 or highest strata in which fuels were present), and by fuel type (for the 0–10 layer only) for use in analyses. Duff biomass values were removed before analysis due to occlusion; duff was not represented in remote sensing point clouds and yet contributed to high total biomass where present. Note that while Sycan Forest I and II data were collected at different times (Table S2), these similar and adjacent sites were combined for analyses.

#### Fuel typing

Simplifying the 19 pre-defined fuel categories into 3 fuel types (shrub, herb and timber litter), plots were organized by their dominant fuel type for analysis using one of two methods. For plots that contained fuel above the 10 cm stratum, typing was done by defining the category with the largest calculated occupied volume as derived from presence/absence observations as dominant. The remaining plots, which only had fuel below this level, were typed using the most abundant category recorded in biomass values (this information was only available for these plots, as upper strata biomass was not sorted). As the forest floor is not well represented in point clouds derived from SfM (Cova et al. 2023) or TLS (Rowell et al. 2020), plots dominated by the timber litter fuel type (and consequently where most or all of the fuel mass was below 10 cm in height) were removed prior to analyses.

#### Statistical analyses

We created Pearson's correlation plots of point cloud metrics and direct field measures (including biomass) for both TLS and SfM using the corrplot package in R (Wei and Simko 2024). Point cloud metrics from both methods were selected for inclusion in linear models based on high Pearson correlation to field-measured biomass above 10 cm. Based on results from earlier work (Cova et al. 2023), we chose to construct univariate linear models to evaluate the ability of each point cloud metric to predict plot biomass, as multivariate models were not shown to improve predictive accuracy in previous work. Model accuracy was evaluated using coefficients of determination ($r^2$) and root mean square error (RMSE). Point cloud metrics from TLS and SfM were compared to their corresponding field-derived metrics using ANOVA (average height and occupied volume). All analyses were performed in R Studio (R Core Team 2024).

Due to known issues with characterizing dense fuels and low sample size, plots with large quantities of coarse woody debris and other high-biomass but low-volume objects were removed before analysis. Because litter and duff layers are subject to occlusion when using photogrammetry and lidar technologies, relationships between point cloud metrics and measured biomass of the forest floor tend to be poorly correlated (Bright et al. 2016). Thus, we used biomass collected above 10 cm from ground level (biomass 10+) as the response variable for all analyses.

## Results

Metrics derived from SfM point clouds and TLS point clouds were comparable and generally performed best on elevated vegetation layers. Average fuel height and occupied volume were the strongest predictors of sampled biomass between 10 and 100 cm in height based on correlation matrices and linear models. (Supplemental Fig. S1). The SfM point cloud metrics that had the strongest correlation to biomass above 10 cm were average height, volume (as calculated using the convex hull function), and hull surface area (Supplemental Fig. S2). Relationships between point cloud metrics and full plot biomass, including forest floor material, were uniformly weak.

### Direct measures comparison

TLS-derived average height was closer to values measured in the field (mean difference: 0.04 m) than SfM-derived height values, although differences between remotely sensed and field-derived metrics were statistically significant for both techniques ($p < 0.01$). SfM scanning methods consistently under-predicted fuel height across both shrub and herb-dominated plots (mean difference: −0.14 m), consistent with Cova and others (2023, Fig. 3). By contrast, SfM point cloud volume metrics better represented field measures of plot volume (mean difference: 0.04 m), while TLS often overpredicted this metric (mean difference: 0.26 m, Fig. 3).

### Global biomass models (all sites)

Based on all sites, predictive models of biomass above 10 cm from TLS and SfM-measured average height were comparable ($r^2 = 0.44$ and 0.49, respectively; Tables 1 and 2; Fig. 4), while SfM models performed slightly better than TLS when using occupied volume ($r^2 = 0.3$ and 0.44, respectively, Fig. 5), hull surface area ($r^2 = 0.25$ and 0.45, respectively) and hull volume ($r^2 = 0.27$ and 0.46, respectively) to predict biomass.

### Site-specific biomass models

While neither scanning method demonstrated improved prediction of plot biomass over the other when the data were examined collectively, there was notable variation in model performance across individual sites. Models with the highest $r^2$ values were generally located in SE flatwood and western pine sites with simple understory structure. Fort Stewart and Tates Hell B models performed well, particularly with SfM-based metrics such as height ($r^2 = 0.84$ and 0.58, respectively) and volume ($r^2 = 0.79$ and 0.64, respectively), while Osceola, LANL, and Sycan Forest sites showed strong model results for most metrics (Tables 1 and 2, Figs. 6 and 7, Figs. S5–6). Forested sites with highly complex understories, such as Hannah Hammock and Aucilla (SfM volume model $r^2 = 0.06$ and 0.3, respectively), or where plots had a substantial herbaceous component (e.g., Blackwater and Hitchiti B) revealed poor relationships (SfM surface area model $r^2 = 0.15$ and 0.19, respectively) between remote-sensing metrics (particularly in SfM models) and measured biomass values. Fuel biomass in grassland sites, such as Glacial Heritage and Tenalquot, were poorly represented by most models created from lidar scanning as well as photogrammetry-generated point clouds. Across all sites, model uncertainty, associated with greater model residual values, increased with biomass.

TLS models that used average vegetation height to predict biomass outperformed SfM models for nearly all sites (Fig. 6). Outcomes of models using occupied volume as a predictor were not conclusively better in SfM models when compared with TLS ones at the site level, despite the improved overall model performance when all sites were combined (Fig. 7). SfM models of hull surface area were improved over those made from TLS point clouds, but grassland sites and most loblolly-sweetgum sites were poorly represented by this metric using either scanning method (Fig. S5). A similar trend was found in models using convex hull volume as a predictor of biomass (Fig. S6).

### Forest floor biomass

As mentioned above, our analyses relied on sampled biomass above 10 cm for comparison with remotely sensed variables, excluding the lowest stratum. Results of Pearson's correlation matrices supported this approach, as poor relationships were evidenced when forest floor biomass was included in total biomass (0 to 100 cm) for comparisons with TLS and SfM-derived metrics ($r$ 0.21–0.3 for TLS metrics, 0.16–0.31 for SfM). In separate analyses, vegetative biomass from the litter layer was found to comprise the vast majority of total plot biomass (Appendix Table S1, Fig. 8). Site-wide mean percentages

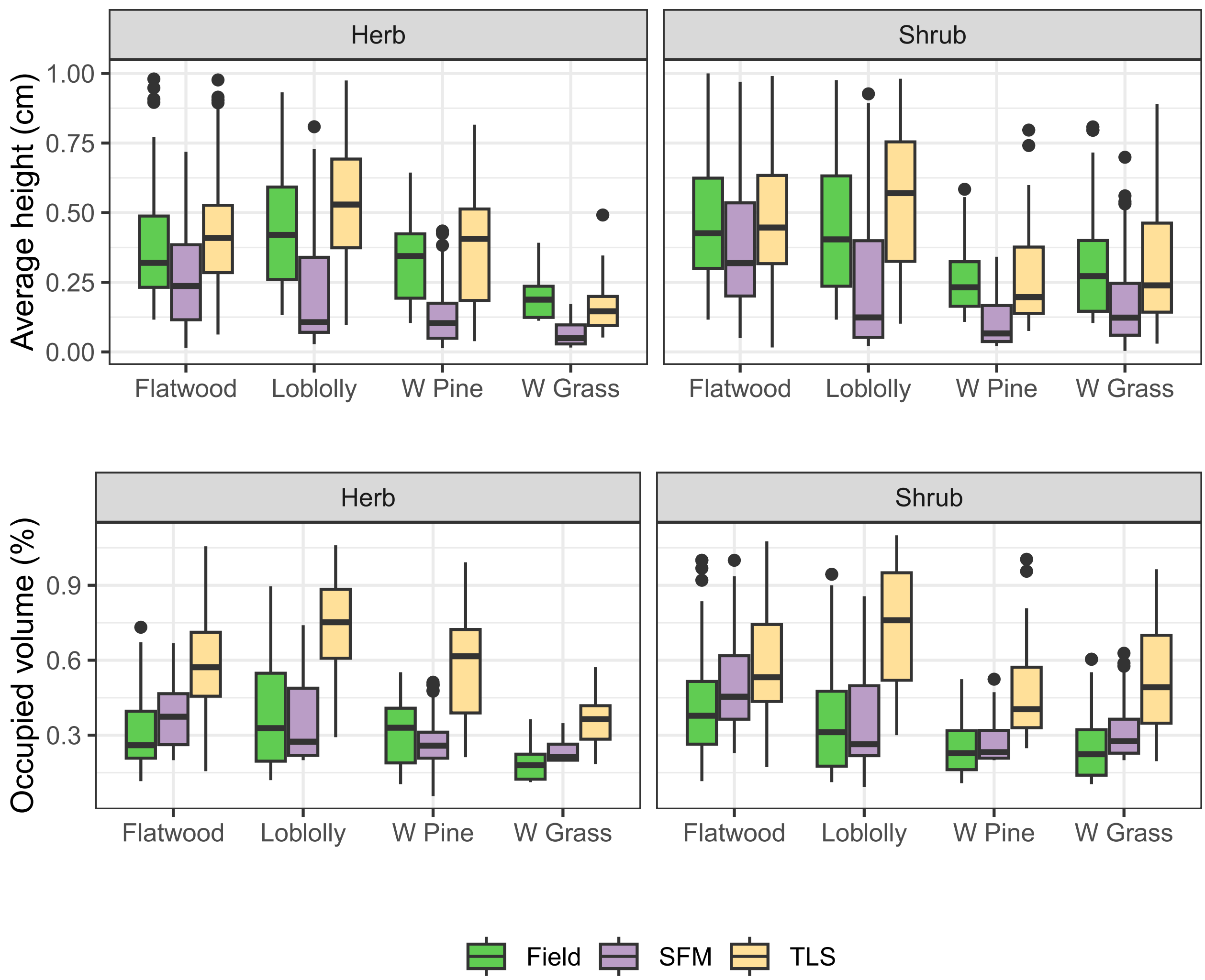


**Fig. 3** Comparison plots of fuel height and occupied volume as measured in the field with average height and volume metrics calculated from TLS (upper) and SfM (lower) point clouds. Data are grouped by dominant fuel type for each plot (herb or shrub) and vegetation type (SE Flatwood, SE Loblolly-sweetgum, Western pine, and Western grassland)

for biomass below 10 cm ranged from 65% of total plot biomass for Hannah Hammock to 97% of biomass for Sycan Grassland.

## Discussion

There is a substantial need for more accurate and geographically distributed 3D fuels data, particularly to support gridded vegetation inputs to physics-based models of fire behavior and effects. Novel methods to characterize fuels for wildland fire decision support and improve biomass estimation are now possible with advances in both active and passive scanning technologies and analyses (Abdollahi and Yebra 2023). Among scanning techniques, TLS and SfM photogrammetry are the most frequently cited as having great potential to reduce or even eliminate the need for meticulous and expensive field sampling of vegetation and fuels (Wallace et al. 2020). Using a large and robust dataset collected from sites distributed across the continental US, we compared these methods for predicting understory fuel biomass across a range of pine forest understory and grassland sites.

As a key input to the calculation of fuel loading and bulk density, biomass is an essential element for predicting fire behavior and smoke production (Rothermel 1972; Scott and Burgan 2005; Pimont et al. 2016; Rowell et al. 2020). Directly measuring fuel biomass in the field, which requires destructive sampling and laboratory analyses, is painstaking and slow. Advances in remote sensing applications have opened possibilities for field measurements that are faster and can be at least partially automated. Work is ongoing to determine which remote sensing methods can accurately predict biomass in the field and train machine learning algorithms with measured

**Table 1** Linear model outputs of field-collected plot biomass above 10 cm modeled using 4 TLS-derived metrics by site ($n = 608$ plots)

| | Average height | | | Occupied volume | | | Surface area | | | Hull volume | | |
|---|---|---|---|---|---|---|---|---|---|---|---|---|
| **Site** | $r^2$ | **RMSE** | ***p*-value** | $r^2$ | **RMSE** | ***p*-value** | $r^2$ | **RMSE** | ***p*-value** | $r^2$ | **RMSE** | ***p*-value** |
| **Southeastern flatwood forests** | | | | | | | | | | | | |
| Tates Hell A | 0.49 | 38.93 | 0.000 | 0.48 | 39.33 | 0.000 | 0.39 | 42.64 | 0.000 | 0.4 | 42.19 | 0.000 |
| Osceola | 0.71 | 34.15 | 0.000 | 0.47 | 45.96 | 0.000 | 0.54 | 42.95 | 0.000 | 0.6 | 40.03 | 0.000 |
| Blackwater | 0.47 | 29.14 | 0.002 | 0.16 | 36.57 | 0.102 | 0.33 | 32.64 | 0.013 | 0.34 | 32.31 | 0.011 |
| Fort Stewart | 0.6 | 19.36 | 0.000 | 0.56 | 20.31 | 0.000 | 0.2 | 27.37 | 0.048 | 0.23 | 26.8 | 0.031 |
| Tates Hell B | 0.57 | 33.96 | 0.000 | 0.57 | 34.04 | 0.000 | 0.5 | 36.82 | 0.000 | 0.53 | 35.65 | 0.000 |
| Aucilla | 0.59 | 59.43 | 0.000 | 0.54 | 62.52 | 0.000 | 0.4 | 71.85 | 0.000 | 0.4 | 71.61 | 0.000 |
| **Loblolly-sweetgum forests** | | | | | | | | | | | | |
| Hannah Hammock | 0.33 | 59.55 | 0.000 | 0.28 | 61.56 | 0.000 | 0.2 | 64.99 | 0.002 | 0.21 | 64.65 | 0.002 |
| Hitchiti B | 0.53 | 28.63 | 0.000 | 0.5 | 29.57 | 0.000 | 0.24 | 36.47 | 0.001 | 0.23 | 36.86 | 0.001 |
| Hitchiti A | 0.45 | 36.14 | 0.000 | 0.47 | 35.49 | 0.000 | 0.23 | 42.66 | 0.001 | 0.25 | 42.05 | 0.001 |
| **Western pine** | | | | | | | | | | | | |
| Lubrecht | 0.54 | 25.65 | 0.000 | 0.36 | 30.3 | 0.000 | 0.42 | 29.06 | 0.000 | 0.46 | 28.01 | 0.000 |
| LANL Forest | 0.65 | 51.49 | 0.000 | 0.71 | 46.8 | 0.000 | 0.51 | 61.6 | 0.000 | 0.55 | 58.46 | 0.000 |
| Methow | 0.35 | 45.29 | 0.000 | 0.4 | 43.39 | 0.000 | 0.3 | 47.18 | 0.001 | 0.32 | 46.29 | 0.000 |
| Sycan Forest | 0.56 | 33.07 | 0.000 | 0.64 | 29.82 | 0.000 | 0.37 | 39.59 | 0.000 | 0.41 | 38.11 | 0.000 |
| **Western grasslands** | | | | | | | | | | | | |
| LANL Grassland | 0.58 | 5.87 | 0.000 | 0.54 | 6.1 | 0.000 | 0.21 | 8.01 | 0.004 | 0.28 | 7.66 | 0.001 |
| Tenalquot | 0.02 | 22.74 | 0.321 | 0.05 | 22.43 | 0.145 | 0.00 | 23.00 | 0.962 | 0.000 | 22.96 | 0.68 |
| Glacial Heritage | 0.00 | 12.18 | 0.821 | 0.00 | 12.17 | 0.728 | 0.00 | 12.16 | 0.646 | 0.000 | 12.18 | 0.772 |
| Sycan Grassland | 0.64 | 1.33 | 0.000 | 0.4 | 1.73 | 0.002 | 0.33 | 1.820 | 0.005 | 0.360 | 1.780 | 0.003 |

**Table 2** Linear model outputs of field-collected plot biomass above 10 cm modeled using 4 SfM-derived metrics by site ($n=595$ plots)

| | Average height | | | Occupied volume | | | Surface area | | | Hull volume | | |
|---|---|---|---|---|---|---|---|---|---|---|---|---|
| **Site** | $r^2$ | **RMSE** | ***p*-value** | $r^2$ | **RMSE** | ***p*-value** | $r^2$ | **RMSE** | ***p*-value** | $r^2$ | **RMSE** | ***p*-value** |
| **Southeastern flatwood forests** | | | | | | | | | | | | |
| Tates Hell A | 0.49 | 39.21 | 0.000 | 0.54 | 37.04 | 0.000 | 0.44 | 40.89 | 0.000 | 0.45 | 40.39 | 0.000 |
| Osceola | 0.6 | 40.08 | 0.000 | 0.63 | 38.22 | 0.000 | 0.63 | 38.54 | 0.000 | 0.66 | 36.69 | 0.000 |
| Blackwater | 0.11 | 38.07 | 0.22 | 0.2 | 36.05 | 0.084 | 0.15 | 37.05 | 0.135 | 0.16 | 36.91 | 0.126 |
| Fort Stewart | 0.84 | 11.93 | 0.000 | 0.79 | 13.51 | 0.000 | 0.64 | 17.84 | 0.000 | 0.75 | 14.68 | 0.000 |
| Tates Hell B | 0.58 | 33.16 | 0.000 | 0.64 | 30.47 | 0.000 | 0.61 | 31.91 | 0.000 | 0.63 | 31.21 | 0.000 |
| Aucilla | 0.32 | 61.72 | 0.000 | 0.3 | 63.02 | 0.000 | 0.33 | 61.28 | 0.000 | 0.36 | 60.29 | 0.000 |
| **Loblolly-sweetgum forests** | | | | | | | | | | | | |
| Hannah Hammock | 0.24 | 64.79 | 0.002 | 0.06 | 71.83 | 0.128 | 0.09 | 70.78 | 0.066 | 0.13 | 69.37 | 0.029 |
| Hitchiti B | 0.28 | 35.65 | 0.000 | 0.14 | 38.77 | 0.013 | 0.14 | 38.91 | 0.015 | 0.11 | 39.45 | 0.029 |
| Hitchiti A | 0.49 | 34.67 | 0.000 | 0.27 | 41.44 | 0.000 | 0.59 | 31.16 | 0.000 | 0.65 | 28.85 | 0.000 |
| **Western pine** | | | | | | | | | | | | |
| Lubrecht | 0.45 | 29.11 | 0.000 | 0.43 | 29.78 | 0.000 | 0.17 | 35.94 | 0.013 | 0.26 | 33.92 | 0.001 |
| LANL Forest | 0.63 | 49.65 | 0.000 | 0.54 | 54.92 | 0.000 | 0.49 | 57.91 | 0.000 | 0.46 | 59.79 | 0.000 |
| Methow | 0.16 | 51.61 | 0.021 | 0.27 | 48.17 | 0.002 | 0.35 | 45.48 | 0.000 | 0.37 | 44.78 | 0.000 |
| Sycan Forest | 0.77 | 21.05 | 0.000 | 0.79 | 20.3 | 0.000 | 0.75 | 21.93 | 0.000 | 0.75 | 22.12 | 0.000 |
| **Western grasslands** | | | | | | | | | | | | |
| LANL Grassland | 0.27 | 8.19 | 0.002 | 0.42 | 7.27 | 0.000 | 0.24 | 8.38 | 0.005 | 0.26 | 8.22 | 0.003 |
| Tenalquot | 0.000 | 22.98 | 0.798 | 0.000 | 23 | 0.969 | 0.000 | 23 | 0.907 | 0.000 | 23 | 0.946 |
| Glacial Heritage | 0.31 | 10.12 | 0.000 | 0.25 | 10.54 | 0.000 | 0.24 | 10.64 | 0.001 | 0.26 | 10.46 | 0.000 |
| Sycan Grassland | 0.12 | 2.09 | 0.115 | 0.28 | 1.9 | 0.012 | 0.33 | 1.83 | 0.005 | 0.34 | 1.8 | 0.004 |

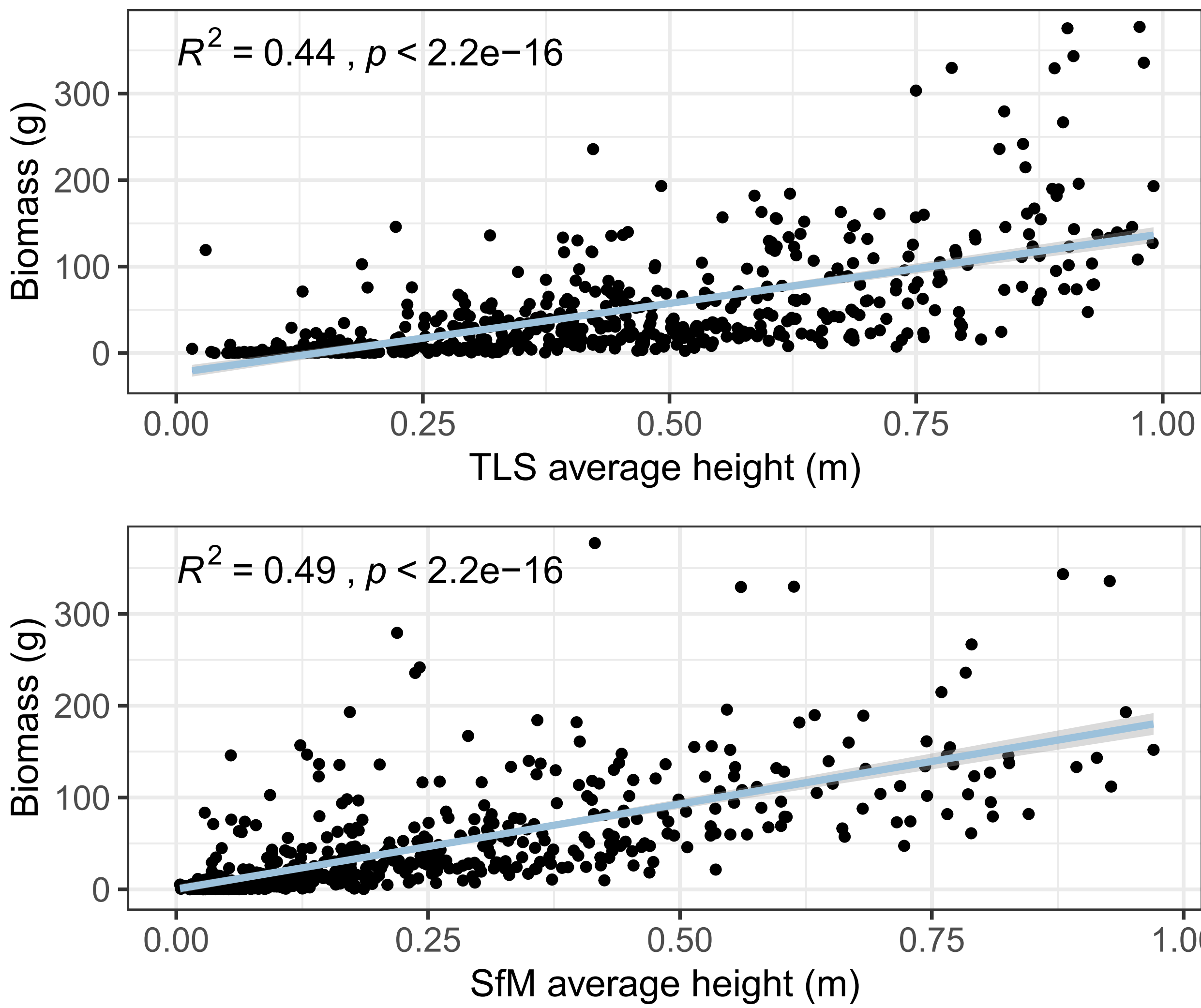


**Fig. 4** TLS and SfM models of average height and field-collected plot biomass above 10 cm

fuel structure and biomass. While previous studies have paired field-based destructive sampling with remote sensing metrics to predict understory biomass (Cooper et al. 2017; Wallace et al. 2017; Hillman et al. 2019; Loudermilk et al. 2023; Arcidiaco et al. 2026), very few have compared commonly used methods while incorporating field observations (Campbell et al. 2023; Batista et al. 2025), and none other (that we are aware of) across highly variable sites. Our results are consistent with previous studies demonstrating moderate relationships between measured values of biomass and point cloud metrics such as height and volume and improved model performance in structurally simpler vegetative environments (Wallace et al. 2017). At sites with lower-stature, more uniform understories (i.e., Fort Stewart, LANL, and Sycan Forests), plot biomass was easier to predict using remotely sensed metrics than the more vegetatively complex sites (i.e., Aucilla, Blackwater, and Hannah Hammock). This is in line with findings from Wallace and others (2017), where the site with the highest biomass and most complex vegetation layers was the most difficult to measure and model using remote sensing techniques. Given the large and varied network of plots we studied (816 destructively sampled plots), with consequently diverse structural characteristics, the high variance of outcomes (from strong to weak model fit) was anticipated.

Because understory fuels are so critical for wildland fire behavior and prescribed fire decision support, tested methods for 3D measurement and mapping of these fuels as inputs into physics-based models of fire behavior and effects are needed (Loudermilk et al. 2014; Rowell et al. 2016; Linn et al. 2020). The fine-scale 3D sampling method employed in this study (Hawley et al. 2018, Prichard et al. in review) represents the type of detailed fuel characterization necessary for the calibration of these fire models to the real-world fuels that burn in wildfires. This

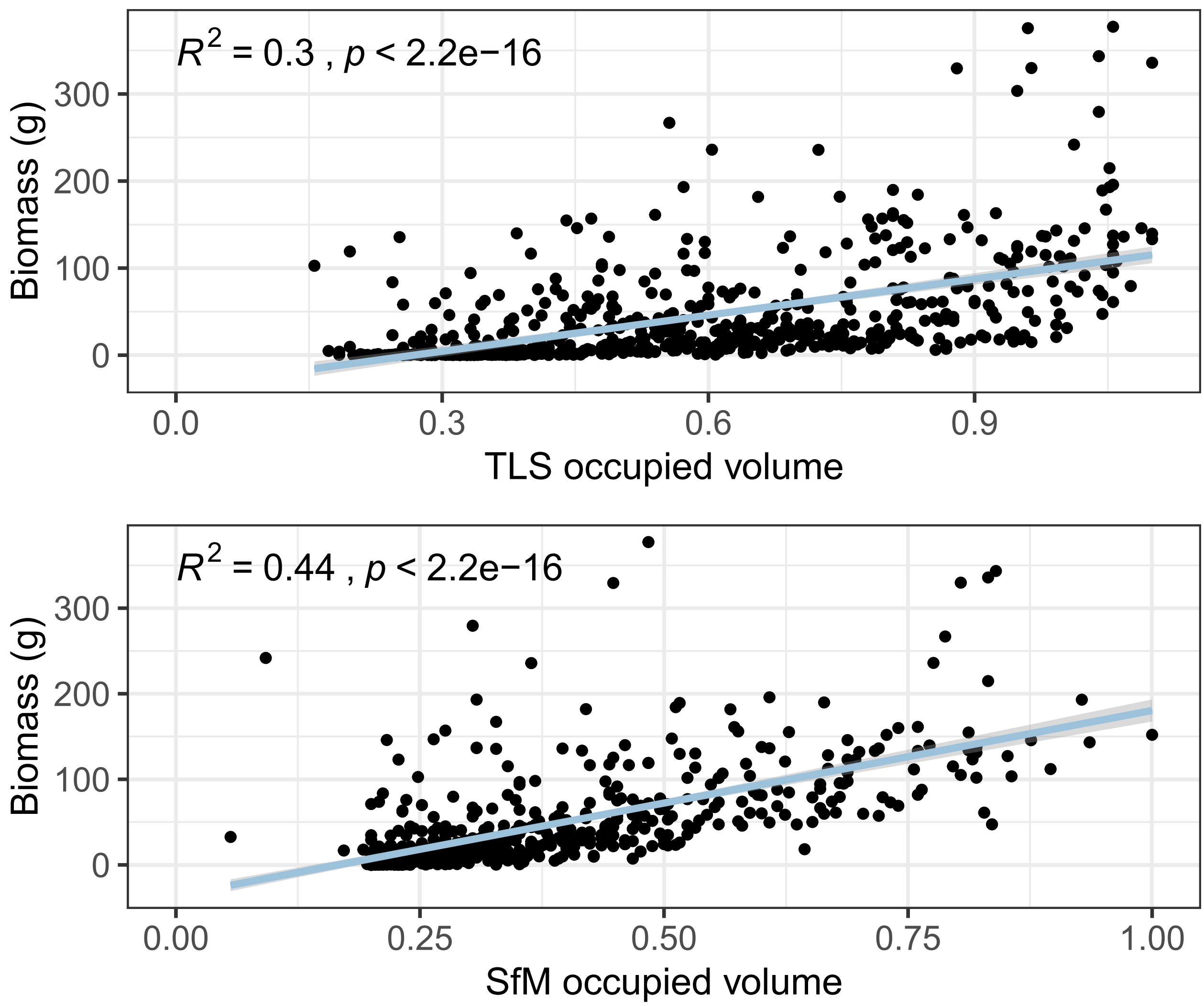


**Fig. 5** TLS and SfM models of occupied volume and field-collected plot biomass above 10 cm

intensive and data-rich sampling framework provides a scalable dataset that could be used in machine learning and AI algorithms to predictively classify and map understory fuels. Our field sampling methods were developed to specifically characterize the fine-scale heterogeneity, structure, and distribution of understory fuels (all of which impact fire flow and thus behavior) on the landscape. While labor-intensive, this sampling and analysis framework presents a viable alternative to the homogeneity and oversimplification of traditional 2D datasets. Additionally, our results suggest that inexpensive photogrammetry technology can be used to create point clouds with accuracy that rivals, and in many cases exceeds, that of more expensive TLS systems.

Similar to Wallace and others (2017), we found that TLS accurately characterizes fine vegetation such as grass blade tips, seed heads, and small leaves, but can also produce erroneous points resulting in “noisy” point clouds. The nature of TLS technology, wherein a large number of sampling points are collected via high-frequency laser pulses, creates a point cloud with many laser returns. This allows TLS to accurately capture narrow and small shapes that contribute to fuel height (such as seed heads or narrow twigs), but can overestimate volume measurements when stray points are included as part of a mass of vegetation (Cooper et al. 2017). Due to this propensity for high-precision structural measurements, including height metrics, it can be difficult to adequately filter out erroneous points (false positives) while maintaining those that represent actual fuels present in the understory (true positives) in the processing stage. By contrast, SfM processing places a smoothing mesh over scanned objects, excluding many stray points: this removes false positives, but also eliminates low-volume

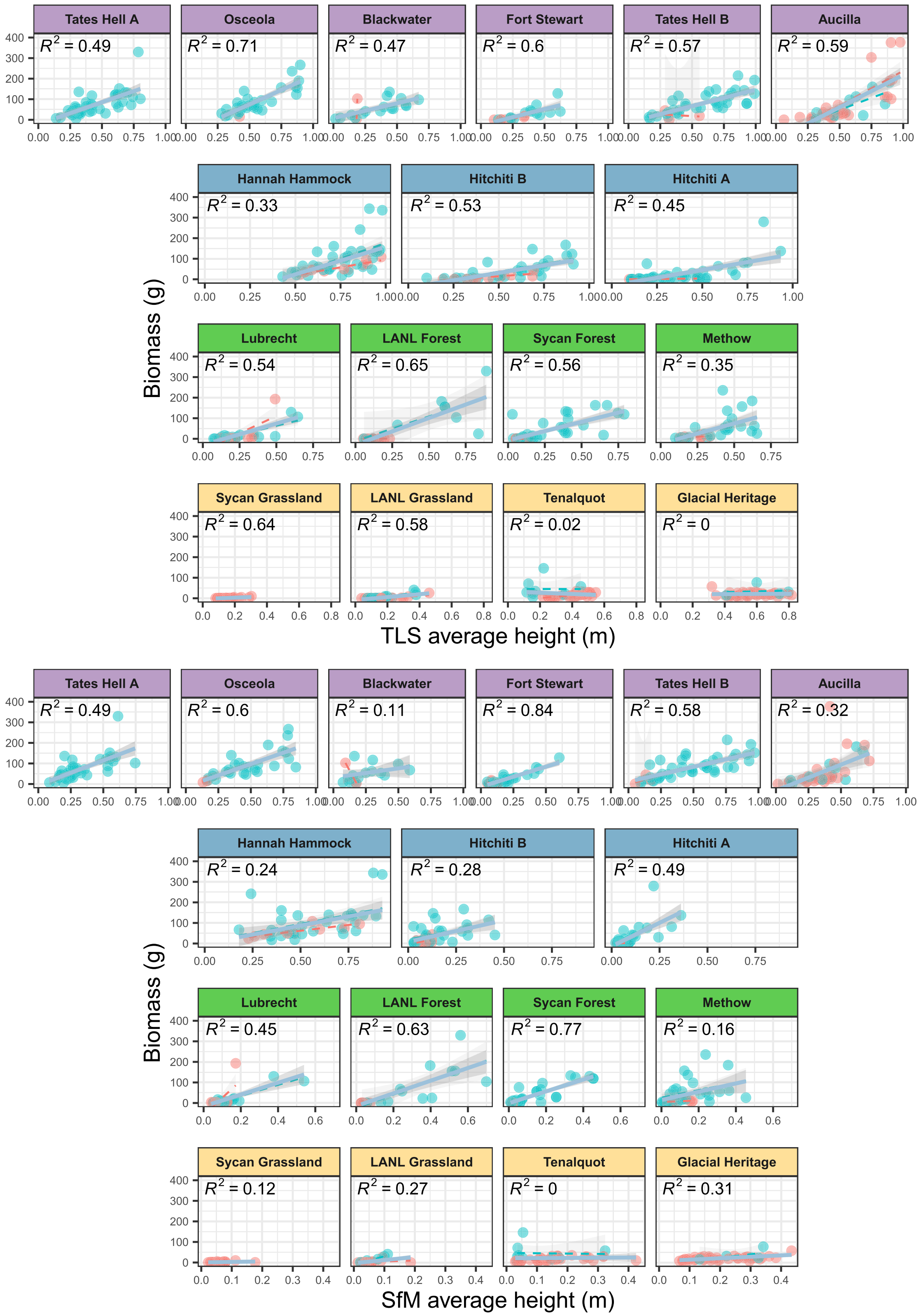


**Fig. 6** TLS and SfM models of average height and field-collected plot biomass above 10 cm. Plots are grouped by vegetation type. Blue points represent shrub-dominated plots, and pink points are herbaceous-dominated plots

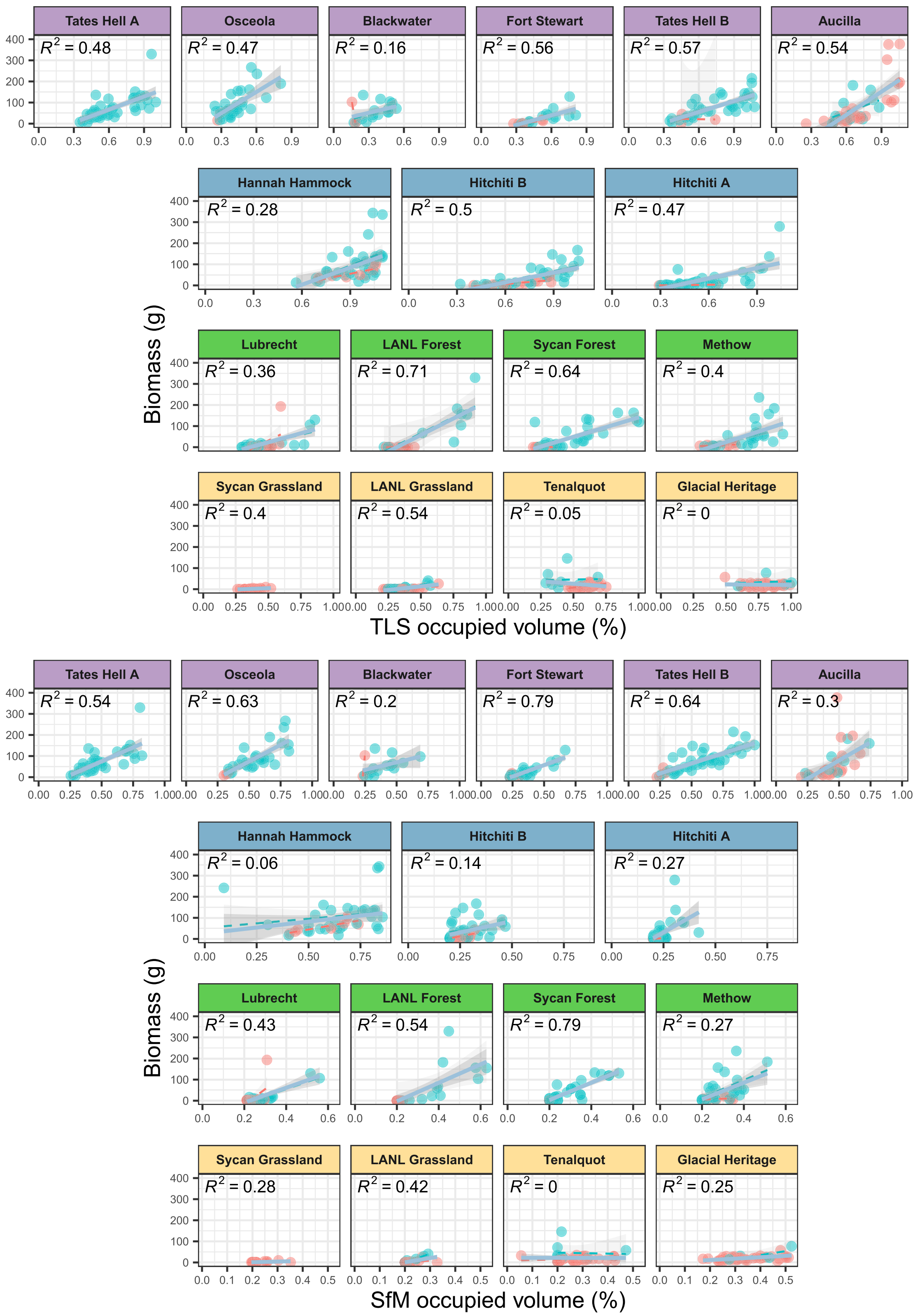


**Fig. 7** TLS and SfM models of occupied volume and field-collected plot biomass above 10 cm. Plots are grouped by vegetation type. Blue points represent shrub-dominated plots, and pink points are herbaceous-dominated plots

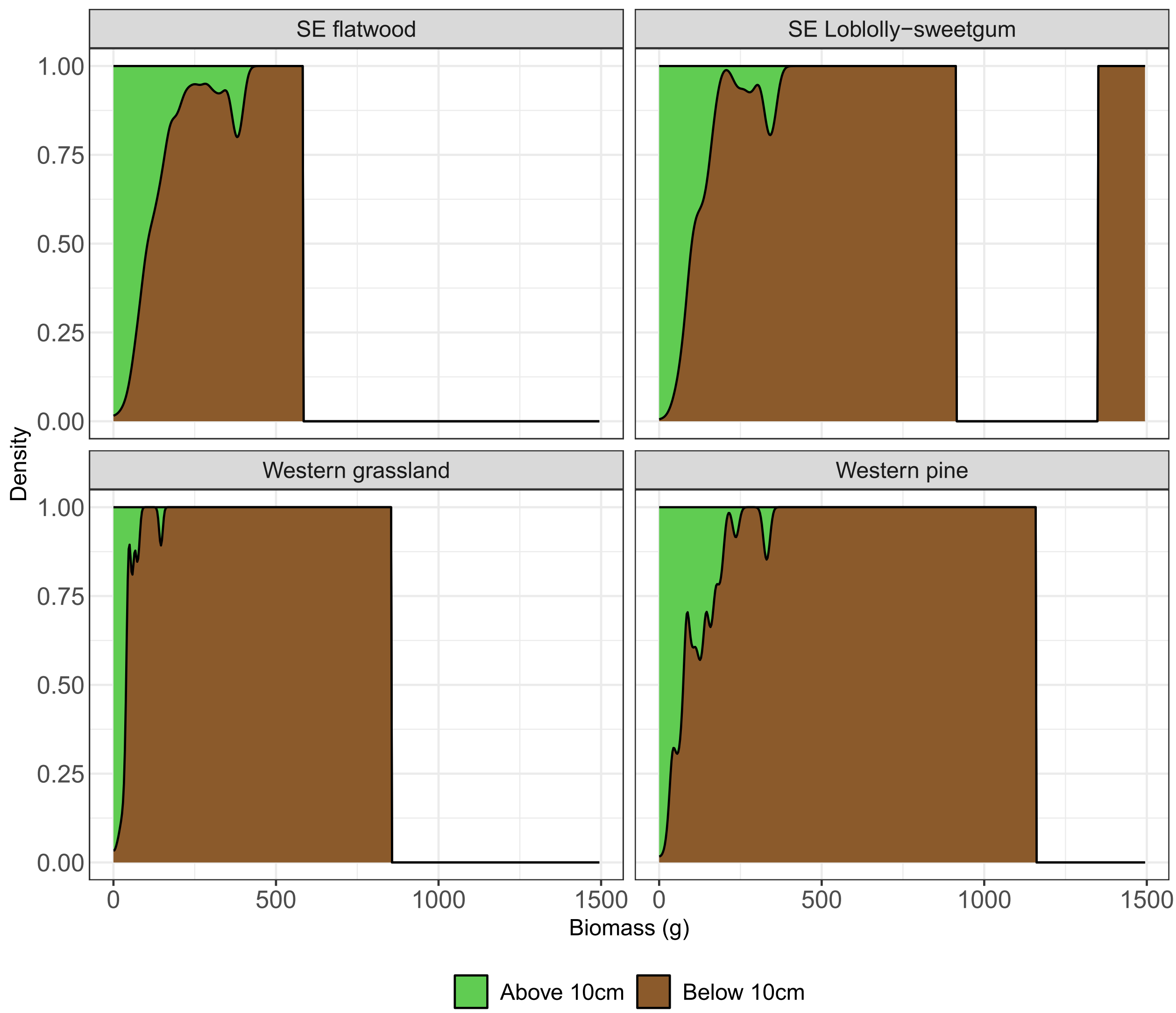


**Fig. 8** Density plot showing distribution of collected plot biomass from both upper strata (above 10 cm, green region) and litter layer (below 10 cm, brown) in each of four vegetation types sampled. Biomass was sampled from above the mineral soil layer up to 1 m above ground level, but duff biomass values were removed prior to analyses

plant parts that are distant from the core of the vegetative sample. Smoothing algorithms bias measurements to uniform textures, rendering a more accurate representation of volume than TLS because fewer disjunct points are included in the final model of the vegetative cluster. However, this function results in the loss of low-volume features that are more accurately captured in TLS point clouds. Other researchers (Bright et al. 2016, Cooper et al. 2017, and Wallace et al. 2020) have documented similar challenges when assessing the fidelity of remote sensing technologies to real-world structures in the field.

Of the fuel types sampled, western grasslands had the weakest relationships between point cloud metrics and measured biomass, regardless of scanning method. Other studies have found similarly weak models in grassland environments (Cooper et al. 2017; Wallace et al. 2020; Enterkine et al. 2025), attributing this to the fineness of these fuels and their density close to the ground, which caused increased occlusion for both types of imagery. Models were particularly poor in tall grassland sites (Tenalquot and Glacial Heritage), whereas stronger relationships were occasionally found in shorter-stature grasslands (LANL and Sycan Grassland). These findings are likely due to the difficulty in capturing fine (particularly tall fine) vegetation with remote sensing methods (Hillman et al. 2019; Wallace et al. 2020), possibly due to lower surface area to produce laser returns in the case of TLS, and the smoothing functions of photogrammetry processing that eliminate disjunct points in SfM-derived point clouds. In addition, wind has more of an effect on scanning in grasslands (with taller grasses more easily disturbed by breezes) as moving vegetation will create variable TLS point clouds with many stray (noise) points, even on days with calm weather (Tilly et al. 2014; Hillman et al. 2019), while any blurry images captured by cameras can be removed before SfM processing occurs, as was done here. Loblolly-sweetgum sites also had poor performance in many models, possibly due to the density of narrow and leafless sweetgum stems that were not accurately captured in SfM or TLS point clouds but had high relative biomass, reflecting similar challenges in modeling shrub fuels using TLS point clouds captured during their leaf-off stage (Maxwell et al. 2023). Sites where the bulk of the biomass was located in the litter layer (below 10 cm) also produced poor model results, as our models were constructed using only the biomass from strata above 10 cm, due to the inherent occlusion in point clouds at this stratum level.

## Limitations and future direction

With over 800 sampled plots in 4 distinct vegetation types of varying fuel structure and loadings, this study begins to address the need for spatial variability and high sampling density that remains lacking in many understory fuel modeling studies (Maxwell et al 2023). While our destructive sampling methods are labor-intensive and time-consuming, these datasets will offer potentially valuable training data for future studies in similar fuel types. Based on our findings, we would recommend some changes to methods for future work that could improve data processing and analyses and possibly yield stronger modeled relationships between point cloud metrics and destructively measured biomass.

During processing of photogrammetry data, we needed to manually delete many still photos from the GoPro video imagery that were blurry, suggesting that setting the camera to take a rapid succession of still photos would result in less processing time than is required for video recordings. Additionally, researchers replicating these methods may want to consider sorting fuel strata above 10 cm for the purpose of fuel typing of entire plots by mass instead of volumetric presence/absence, as was done in this study. For more complex modeling processes—ones that incorporate intrinsic fuel properties, for example—characterizing all plant parts by species (instead of grouping into category as was done here) within each clip plot would be necessary. The inability of either TLS or SfM to accurately predict biomass of the litter layer (below 10 cm) is an ongoing issue for all forms of remote sensing, as occlusion in this layer often prevents accurate representation. This is a concern for fire behavior and particularly smoke production models, as litter and duff contain high concentrations of forest biomass, but are not well characterized in remote sensing fuel models (Rowell et al. 2020; Cova et al. 2023; Enterkine et al. 2025). One recent study had success in modeling plot biomass that included the litter layer using a multiple linear regression approach (Loudermilk et al. 2023); this may be partially due to the addition of more metrics, as well as to the simple, short stature fuels of the single field location studied (Fort Stewart). Our objective of comparing metrics across 18 sites with variable fuels did not allow for customized models for each site, but our simpler analysis did produce strong models for this location. Given the known limitations of remote sensing for the lowest fuel profiles, we would recommend separate studies that involve high intensity sampling of litter and duff biomass to facilitate model development between overstory tree crowns and shrubs with litter and duff distributions and depths (sensu Sanchez-Lopez et al. 2026).

The potential of next-generation fire behavior models to assist with operational decision support, particularly in prescribed fire operations, is promising in that these models are able to represent fine-scale heterogeneity of fuels, fire behavior, and effects (Linn et al. 2002, 2020; Mell et al. 2007). In order for physics-based models to realize their full potential to predict fire behavior, spread, intensity, and resultant smoke production, datasets of the type described here must be made available to researchers. Our scalable dataset was designed to test how close-range remote sensing could be used to measure understory structure and predict biomass across a range of pine forests and grasslands, which are the most common fuel types within US prescribed fire programs. The level of detail presented in the full dataset (https://wfsi-data.org) is highly consequential for fire modeling, as it captures the structure and arrangement of fuels on a fine scale, including characterizing gaps in voxelized fuels that are important for cellular automata models such as QUIC-fire. Using gridded 3D maps like these, researchers can create new metrics that quantify fuel properties and spatial characteristics important to heat release and fire spread. This will provide useful interpretation for managers, particularly in fuels reduction and prescribed fire programs.

## Supplementary Information

The online version contains supplementary material available at https://doi.org/10.1186/s42408-026-00503-6.

Supplementary Material 1: Figure S1: Correlation Matrix for seven TLS metrics, three field-measured metrics, and 2 measures of plot biomass. Figure S2: Correlation Matrix for seven SfM metrics, three field-measured metrics, and 2 measures of plot biomass. Figure S3: TLS and SfM models of hull surface area and field-collected plot biomass above 10 cm. Figure

S4: TLS and SfM models of hull volume and field-collected plot biomass above 10 cm. Figure S5: TLS and SfM models of hull surface area and field-collected plot biomass above 10 cm. Plots are grouped by vegetation type. Blue points represent shrub-dominated plots, and pink points are herbaceous-dominated plots. Figure S6: TLS and SfM models of hull volume and field-collected plot biomass above 10 cm. Plots are grouped by vegetation type. Blue points represent shrub-dominated plots, and pink points are herbaceous-dominated plots. Table S1: Percentage of biomass per plot in the 0–10 cm strata, above 10 cm, and mean total biomass per site. Table S2: 3D Fuels study site descriptions and sampling dates. TSF = time since fire. As western sites were not as frequently burned as eastern ones, we used rough estimates of site-level fuel biomass (low–high) to stratify our sampling sites.

**Acknowledgements**
We thank Danielle Christianson, Christie Hawley, James Furman, J. Kevin Hiers, Scott Pokwinski, Brett Williams, Jonathan Bachelor and Ben Bright for their support and guidance on this project. We thank our field and laboratory staff for their hard work and dedication, particularly field supervisor Jim Cronan, as well as Nick Tripodi, Lindsay Lascheck, Maddy Hallet, Teagan Darmody, Matt Nolasco, Mason Patterson, Henry Gould, Kate Patronik, Grace Swan-Streepy, Jordan Hilton, Sophia Boyd, Jane Wynne, and Caitlyn Bell. We also thank the managers and experts at Glacial Heritage and Tenalquot Preserves, Blackwater and Tates Hell State Forests, Hitchiti and Lubrecht Experimental Forests, Los Alamos National Laboratory, Middle Aucilla Conservation Area, Tall Timbers Research Station, Fort Stewart, Osceola National Forests, and Methow Wildlife Area. We would also like to thank two anonymous reviewers for their helpful comments, which greatly improved an earlier version of this manuscript.

**Authors' contributions**
SJP and ER contributed to study design. DN, JT, PE and BD contributed to data collection, management, processing and QAQC. DN and PE supported database development and design. DN lead data analysis and writing, with significant contribution from SJP and GRC. All authors read and approved the final manuscript.

**Funding**
This study was funded by the US Department of Defense Strategic and Environmental Research and Development Program (SERDP Projects # RC19-1064 and RC20-1346). This research was supported (in part) by the US Department of Agriculture, Forest Service. Any use of trade, firm, or product names is for descriptive purposes only and does not imply endorsement by the US government.

**Data availability**
The datasets for this study are open source and are being archived with the Wildland Fire Science Initiative data repository (https://wfsi-data.org, doi.org/https://doi.org/10.60594/W4W016), including project metadata, methods documentation, and data libraries. Data processing and analysis scripts are archived and publicly available on GitHub (https://github.com/uw-flame-lab/3D_Fuels_PUBLIC/).

## Declarations

**Ethics approval and consent to participate**
n/a.

**Consent for publication**
N/a.

**Competing interests**
The authors declare no competing interests.

**Author details**
[1]School of Environmental and Forest Sciences, University of Washington, Seattle, WA, USA. [2]California Air Resources Board, Sacramento, CA, USA.

Received: 27 January 2026 Accepted: 29 April 2026
Published online: 16 May 2026

**References**

Abdollahi, A., and M. Yebra. 2023. Forest fuel type classification: Review of remote sensing techniques, constraints and future trends. *Journal of Environmental Management* 342 : 118315.

Albini, F. A. 1976. Estimating wildfire behavior and effects. Page 92. General Technical Report, Department of Agriculture, Forest Service, Intermountain Forest and Range Experiment Station, Ogden, UT.

Arcidiaco, L., M. Rogai, G. De Luca, C. Nati, A. Berton, D. Pellegrini, and G. Picchi. 2026. Point cloud density approach to characterize and estimate shrub fuel load in the Mediterranean environments using mobile laser scanning. *Computers and Electronics in Agriculture* 241 : 111265.

Atchley, A. L., R. Linn, A. Jonko, C. Hoffman, J. D. Hyman, F. Pimont, C. Sieg, and R. S. Middleton. 2021. Effects of fuel spatial distribution on wildland fire behaviour. *International Journal of Wildland Fire* 30:179.

Batista, E.K.L., A.T. Hudak, J.W. Atkins, E.N. Broadbent, K.M. Brock, M.J. Campbell, N. Sánchez-López, M.B. Schlickmann, F. Mauro, A. Susaeta, et al. 2025. Comparing terrestrial and mobile laser scanning approaches for multilayer fuel load prediction in the Western United States. *Remote Sensing* 17: 2757.

Bright, B. C., E. L. Loudermilk, S. M. Pokswinski, A. T. Hudak, and J. J. O'Brien. 2016. Introducing close-range photogrammetry for characterizing forest understory plant diversity and surface fuel structure at fine scales. *Canadian Journal of Remote Sensing* 42:460–472.

Calders, K., J. Adams, J. Armston, H. Bartholomeus, S. Bauwens, L. P. Bentley, J. Chave, F. M. Danson, M. Demol, M. Disney, R. Gaulton, S. M. Krishna Moorthy, S. R. Levick, N. Saarinen, C. Schaaf, A. Stovall, L. Terryn, P. Wilkes, and H. Verbeeck. 2020. Terrestrial laser scanning in forest ecology: Expanding the horizon. *Remote Sensing of Environment* 251 : 112102.

Campbell, M. J., J. F. Eastburn, K. A. Mistick, A. M. Smith, and A. E. Stovall. 2023. Mapping individual tree and plot-level biomass using airborne and mobile lidar in piñon-juniper woodlands. *International Journal of Applied Earth Observation and Geoinformation* 118 : 103232.

Cooper, S.D., D.P. Roy, C.B. Schaaf, and I. Paynter. 2017. Examination of the potential of terrestrial laser scanning and structure-from-motion photogrammetry for rapid nondestructive field measurement of grass biomass. *Remote Sensing* 9: 531.

Cova, G. R., S. J. Prichard, E. Rowell, B. Drye, P. Eagle, M. C. Kennedy, and D. G. Nemens. 2023. Evaluating close-range photogrammetry for 3d understory fuel characterization and biomass prediction in pine forests. *Remote Sensing* 15 : 4837.

Enterkine, J., A. Hojatimalekshah, M. Vermillion, T. Van Der Weide, S.A. Arispe, W.J. Price, A. Hulet, and N.F. Glenn. 2025. Voxel volumes and biomass: Estimating vegetation volume and litter accumulation of exotic annual grasses using automated ultra-high-resolution SfM and advanced classification techniques. *Ecology and Evolution* 15: e70883.

Finney, M.A., S.S. McAllister, T.P. Grumstrup, and J.M. Forthofer. 2021. *Wildland Fire Behavior: dynamics, principles and processes*. Australia: CSIRO Publishing.

Ganteaume, A., B. Guillaume, B. Girardin, and F. Guerra. 2023. CFD modelling of WUI fire behaviour in historical fire cases according to different fuel management scenarios. *International Journal of Wildland Fire* 32:363–379.

Hawley, C.M., E.L. Loudermilk, E.M. Rowell, and S. Pokswinski. 2018. A novel approach to fuel biomass sampling for 3D fuel characterization. *MethodsX* 5: 1597–1604.

Hiers, J. K., J. J. O'Brien, R. J. Mitchell, J. M. Grego, and E. L. Loudermilk. 2009. The wildland fuel cell concept: An approach to characterize fine-scale variation in fuels and fire in frequently burned longleaf pine forests. *International Journal of Wildland Fire* 18:315.

Hillman, S., L. Wallace, K. Reinke, B. Hally, S. Jones, and D. S. Saldias. 2019. A method for validating the structural completeness of understory vegetation models captured with 3D remote sensing. *Remote Sensing* 11 : 2118.

Hudak, A.T., A. Kato, B.C. Bright, E.L. Loudermilk, C. Hawley, J.C. Restaino, R.D. Ottmar, G.A. Prata, C. Cabo, S.J. Prichard, E.M. Rowell, and D.R. Weise. 2020. Towards spatially explicit quantification of pre-and postfire fuels and fuel consumption from traditional and point cloud measurements. *Forest Science* 66: 428–442.

Keane, R.E. 2015. *Wildland fuel fundamentals and applications*. Cham, Switzerland: Springer International Publishing.

Lecigne, B., S. Delagrange, and C. Messier. 2018. Exploring trees in three dimensions: VoxR, a novel voxel-based R package dedicated to analysing the complex arrangement of tree crowns. *Annals of Botany* 121: 589–601.

Linn, R.R., J. Reisner, J.J. Colman, and J. Winterkamp. 2002. Studying wildfire behavior using FIRETEC. *International Journal of Wildland Fire* 11: 233.

Linn, R. R., S. Goodrick, S. Brambilla, M. Brown, R. Middleton, J. O'Brien, and J. Hiers. 2020. QUIC-fire: A fast-running simulation tool for prescribed fire planning. *Environmental Modelling & Software* 125 : 104616.

Loudermilk, E.L., J.J. O'Brien, R.J. Mitchell, W.P. Cropper, J.K. Hiers, S. Grunwald, J. Grego, and J.C. Fernandez-Diaz. 2012. Linking complex forest fuel structure and fire behaviour at fine scales. *International Journal of Wildland Fire* 21: 882–893.

Loudermilk, E. L., G. L. Achtemeier, J. J. O'Brien, J. K. Hiers, and B. S. Hornsby. 2014. High-resolution observations of combustion in heterogeneous surface fuels. *International Journal of Wildland Fire* 23:1016.

Loudermilk, E.L., J.K. Hiers, and J.J. O'Brien. 2018. Chapter 6: The Role of Fuels for Understanding Fire Behavior and Fire Effects. In *Ecological Restoration and Management of Longleaf Pine*, 107–122.

Loudermilk, E. L., J. J. O'Brien, S. L. Goodrick, R. R. Linn, N. S. Skowronski, and J. K. Hiers. 2022. Vegetation's influence on fire behavior goes beyond just being fuel. *Fire Ecology* 18 (9) : s42408-022-00132–9.

Loudermilk, E. L., S. Pokswinski, C. M. Hawley, A. Maxwell, M. R. Gallagher, N. S. Skowronski, A. T. Hudak, C. Hoffman, and J. K. Hiers. 2023. Terrestrial laser scan metrics predict surface vegetation biomass and consumption in a frequently burned southeastern US ecosystem. *Fire* 6:151.

Maxwell, A. E., M. R. Gallagher, N. Minicuci, M. S. Bester, E. L. Loudermilk, S. M. Pokswinski, and N. S. Skowronski. 2023. Impact of reference data sampling density for estimating plot-level average shrub heights using terrestrial laser scanning data. *Fire* 6 : 98.

Mell, W., M. A. Jenkins, J. Gould, and P. Cheney. 2007. A physics-based approach to modelling grassland fires. *International Journal of Wildland Fire* 16:1–22.

Mueller, E. V., N. S. Skowronski, K. L. Clark, M. R. Gallagher, W. E. Mell, A. Simeoni, and R. M. Hadden. 2021. Detailed physical modeling of wildland fire dynamics at field scale - An experimentally informed evaluation. *Fire Safety Journal* 120 : 103051.

Piermattei, L., W. Karel, D. Wang, M. Wieser, M. Mokroš, P. Surový, M. Koreň, J. Tomaštík, N. Pfeifer, and M. Hollaus. 2019. Terrestrial structure from motion photogrammetry for deriving forest inventory data. *Remote Sensing* 11:950.

Pimont, F., R. Parsons, E. Rigolot, F. De Coligny, J.-L. Dupuy, P. Dreyfus, and R.R. Linn. 2016. Modeling fuels and fire effects in 3D: Model description and applications. *Environmental Modelling & Software* 80: 225–244.

Prichard, S.J., M.C. Kennedy, A.G. Andreu, P.C. Eagle, N.H. French, and M. Billmire. 2019. Next-generation biomass mapping for regional emissions and carbon inventories: Incorporating uncertainty in wildland fuel characterization. *Journal of Geophysical Research: Biogeosciences* 124: 3699–3716.

R Core Team. 2024. *R, A language and environment for statistical computing*. Vienna, Austria: R Foundation for Statistical Computing.

Rothermel, R. 1972. *A mathematical model for predicting fire spread in wildland fuels*, 40. Ogden, UT: U.S. Department of Agriculture, Forest Service, Intermountain Forest and Range Experiment Station.

Roussel, J.-R., D. Auty, N.C. Coops, P. Tompalski, T.R.H. Goodbody, A.S. Meador, J.-F. Bourdon, F. De Boissieu, and A. Achim. 2020. lidR: An R package for analysis of airborne laser scanning (ALS) data. *Remote Sensing of Environment* 251: 112061.

Rowell, E.M., E.L. Loudermilk, C. Seielstad, and J.J. O'Brien. 2016. Using simulated 3D surface fuelbeds and terrestrial laser scan data to develop inputs to fire behavior models. *Canadian Journal of Remote Sensing* 42: 443–459.

Rowell, E.M., E.L. Loudermilk, C. Hawley, S. Pokswinski, C. Seielstad, Ll.. Queen, J.J. O'Brien, A.T. Hudak, S. Goodrick, and J.K. Hiers. 2020. Coupling terrestrial laser scanning with 3D fuel biomass sampling for advancing wildland fuels characterization. *Forest Ecology and Management* 462: 117945.

Sánchez-López, N., Hudak, A.T., Callaham, M.A., Taylor, M.K., Viskari, T., Bright, B.C., Bigelow, S., Prichard, S.,Loudermilk, E.L., Boschetti, L. and Hawley, C., 2026. Coupling duff development with tree litter and downed fuel inputs, decomposition and fire consumption in a long-term prescribed fire experiment in Florida. *International Journal of Wildland Fire* 35(2): p.WF24205.

Scott, J. H., and R. E. Burgan. 2005. *Standard fire behavior fuel models: A comprehensive set for use with Rothermel's surface fire spread model*, RMRS-GTR-153. Ft. Collins, CO: U.S. Department of Agriculture, Forest Service, Rocky Mountain Research Station.

Tenny, J. T., T. T. Sankey, S. M. Munson, A. J. Sánchez Meador, and S. J. Goetz. 2025. Canopy and surface fuels measurement using terrestrial lidar single-scan approach in the Mogollon Highlands of Arizona. *International Journal of Wildland Fire* 34 : WF24221.

Tilly, N., D. Hoffmeister, Q. Cao, S. Huang, V. Lenz-Wiedemann, Y. Miao, and G. Bareth. 2014. Multitemporal crop surface models: Accurate plant height measurement and biomass estimation with terrestrial laser scanning in paddy rice. *Journal of Applied Remote Sensing* 8 : 083671–083671.

Wallace, L., S. Hillman, K. Reinke, and B. Hally. 2017. Non-destructive estimation of above-ground surface and near-surface biomass using 3D terrestrial remote sensing techniques. *Methods in Ecology and Evolution* 8:1607–1616.

Wallace, L., B. Hally, S. Hillman, S. D. Jones, and K. Reinke. 2020. Terrestrial image-based point clouds for mapping near-ground vegetation structure: Potential and limitations. *Fire* 3:59.

## Publisher's Note